

École doctorale n° 364 : Sciences Fondamentales et Appliquées

## Doctorat ParisTech

### THÈSE

pour obtenir le grade de docteur délivré par

**L'École Nationale Supérieure des Mines de Paris**

**Spécialité doctorale “Science et Génie des Matériaux”**

*présentée et soutenue publiquement par*

**Ali SAAD**

le xx mai 2015

## NUMERICAL MODELLING OF MACROSEGREGATION INDUCED BY SOLIDIFICATION SHRINKAGE IN A LEVEL SET APPROACH

Directeurs de thèse: **Michel BELLET**  
**Charles-André GANDIN**

### Jury

<b>M. Blablabla</b> ,	Professeur, MINES ParisTech	Rapporteur
<b>M. Blablabla</b> ,	Professeur, Arts Et Métiers ParisTech	Rapporteur
<b>M. Blablabla</b> ,	Chargé de recherche, ENS Cachan	Examinateur
<b>M. Blablabla</b> ,	Danseuse, en freelance	Examinateur
<b>M. Blablabla</b> ,	Ingénieur, MIT	Examinateur

T  
H  
E  
S  
S



# Contents

<b>1 General Introduction</b>	<b>1</b>
1.1 Casting defects . . . . .	1
1.2 Macrosegregation . . . . .	4
1.2.1 Causes . . . . .	4
1.2.2 Examples . . . . .	6
1.3 Industrial Worries . . . . .	8
1.4 Project context and objectives . . . . .	9
1.4.1 Context . . . . .	9
1.4.2 Objectives and outline . . . . .	10
<b>2 Modelling Review</b>	<b>13</b>
2.1 Modelling macrosegregation . . . . .	14
2.1.1 Dendritic growth . . . . .	14
2.1.2 Mush permeability . . . . .	14
2.1.3 Microsegregation . . . . .	16
2.1.4 Macroscopic solidification model: monodomain . . . . .	18
2.2 Eulerian and Lagrangian motion description . . . . .	24
2.2.1 Overview . . . . .	24
2.2.2 Interface capturing . . . . .	26
2.3 Solidification models with level set . . . . .	26
2.4 The level set method . . . . .	27
2.4.1 Diffuse interface . . . . .	28
2.4.2 Mixing Laws . . . . .	29
2.5 Interface motion . . . . .	31
2.5.1 Level set transport . . . . .	32
2.5.2 Level set regularisation . . . . .	33
<b>3 Energy balance with thermodynamic tabulations</b>	<b>39</b>
3.1 State of the art . . . . .	40
3.2 Thermodynamic considerations . . . . .	40
3.2.1 Volume averaging . . . . .	40

## Contents

---

3.2.2	The temperature-enthalpy relationship . . . . .	41
3.2.3	Tabulation of properties . . . . .	42
3.3	Numerical method . . . . .	43
3.3.1	Enthalpy-based approach . . . . .	47
3.3.2	Temperature-based approach . . . . .	47
3.3.3	Convergence . . . . .	48
3.4	Validation . . . . .	49
3.4.1	Pure diffusion . . . . .	49
3.4.2	Convection and diffusion . . . . .	52
3.5	Application: multicomponent alloy solidification . . . . .	55
3.5.1	Tabulations . . . . .	57
3.5.2	Discussion . . . . .	58
<b>4</b>	<b>Macrosegregation with liquid metal motion</b>	<b>63</b>
4.1	Introduction . . . . .	64
4.2	Numerical treatment . . . . .	64
4.2.1	Stable mixed finite elements . . . . .	64
4.2.2	Variational multiscale (VMS) . . . . .	64
4.3	VMS solver . . . . .	65
4.4	Computational stability . . . . .	66
4.4.1	CFL condition . . . . .	66
4.4.2	Integration order . . . . .	66
4.5	Application to multicomponent alloys . . . . .	66
4.5.1	Results . . . . .	68
4.6	Macroscopic freckle prediction . . . . .	69
4.6.1	Introduction . . . . .	71
4.6.2	Experimental work . . . . .	72
4.6.3	Macroscopic scale simulations . . . . .	72
4.7	Meso-Macro freckle prediction . . . . .	79
4.7.1	Numerical method . . . . .	79
4.7.2	Configuration . . . . .	81
4.7.3	Effect of vertical temperature gradient . . . . .	84
4.7.4	Effect of cooling rate . . . . .	86
4.7.5	Effect of lateral temperature gradient . . . . .	88
4.7.6	Mono-grain freckles . . . . .	90
<b>5</b>	<b>Macrosegregation with solidification shrinkage</b>	<b>91</b>
5.1	Introduction . . . . .	92
5.2	FE model: Metal . . . . .	92
5.2.1	Mass and momentum conservation . . . . .	94
5.2.2	Energy conservation . . . . .	95

## Contents

---

5.2.3	Species conservation . . . . .	97
5.3	FE model: Air . . . . .	99
5.3.1	Mass and momentum conservation . . . . .	100
5.3.2	Energy conservation . . . . .	100
5.3.3	Species conservation . . . . .	100
5.4	FE monolithic model . . . . .	100
5.4.1	Permeability mixing . . . . .	100
5.4.2	Model equations . . . . .	101
5.4.3	Interface treatment . . . . .	101
5.5	Shrinkage without macrosegregation . . . . .	103
5.5.1	Al-7wt% Si . . . . .	104
5.5.2	Pb-3wt% Sn . . . . .	104
5.6	Shrinkage with macrosegregation . . . . .	104
5.6.1	Al-7wt% Si . . . . .	104
5.6.2	Pb-3wt% Sn . . . . .	104
<b>Bibliography</b>		<b>105</b>

## **Contents**

---

---

<b>Acronym</b>	<b>Standing for</b>
ALE	Arbitrary Lagrangian-Eulerian
BTR	Brittleness temperature range
CCEMLCC	Chill Cooling for the Electro-Magnetic Levitator in relation with Continuous Casting of steel
CEMEF	Center for Material Forming
CSF	Continuum Surface Force
DLR	Deutsches Zentrum für Luft- und Raumfahrt
EML	Electromagnetic levitation
ESA	European Space Agency
FEM	Finite Element Method
GMAW	Gas Metal Arc Welding
ISS	International Space Station
IWT	Institut für Werkstofftechnik
LHS	Left Hand Side
LSM	Level set method
MAC	Marker-and-cell
MIN	Mini-element
PF	Phase field
RHS	Right Hand Side
RUB	Ruhr Universität Bochum
RVE	Representative Elementary Volume
SCPG	Shock Capturing Petrov-Galerkin
SUPG	Streamline Upwind Petrov-Galerkin
VMS	Variational MultiScale
VOF	Volume Of Fluid

---

## **Contents**

---

# Chapter 1

## General Introduction

Casting is one the earliest production techniques created by human civilisation since the Bronze Age, dated to circa 3000 BC. From ancient swords to nowadays toys, the need for alloys has never decreased. The key phenomenon behind this technique is solidification, or the transformation of matter from liquid to solid state. With this phase change, many phenomena, not visible to the naked eye, take place with a very complex interaction, in order to form a solid. However, the combination of thermal phenomena, like release of latent heat of solidification, and chemical phenomena like redistribution of chemical element atoms (also known as solute) with other atoms, often lead to *segregation*. The origins of this word from Latin, *segregatus*, has a social meaning of "separating a group from the dominant majority", while in metallurgy it means a non uniform distribution of chemical species. Depending on the scale, we may speak of *microsegregation* when the heterogeneity spans some few hundred microns, whereas the term *macrosegregation* refers to a much coarser length scale, ranging from some millimetres to some meters ! The final solid structure is has intrinsic thermophysical and thermomechanical properties directly influenced by the segregation pattern. In casting processes, such as continuous casting ([fig. 1.1](#)) and ingot casting, it is crucial to apprehend these intricate phenomena leading to macrosegregation as well as the influence on the final product, at each step of the process.

### 1.1 Casting defects

Undesired effects are inevitable in any industrial process. More importantly, a lot of defects in the casting industry can be disastrous in some situations where the cast product is not serviceable and hence rejected. This leads to a systematic product recycling, i.e. the product is ditched to be reheated, remelted and then cast again. From an economic point view, the operation is expensive timewise and profitwise. Understanding and preventing defects when possible, is thus crucial in the casting industry. We briefly list hereafter the main encountered defects.

## Chapter 1. General Introduction

---

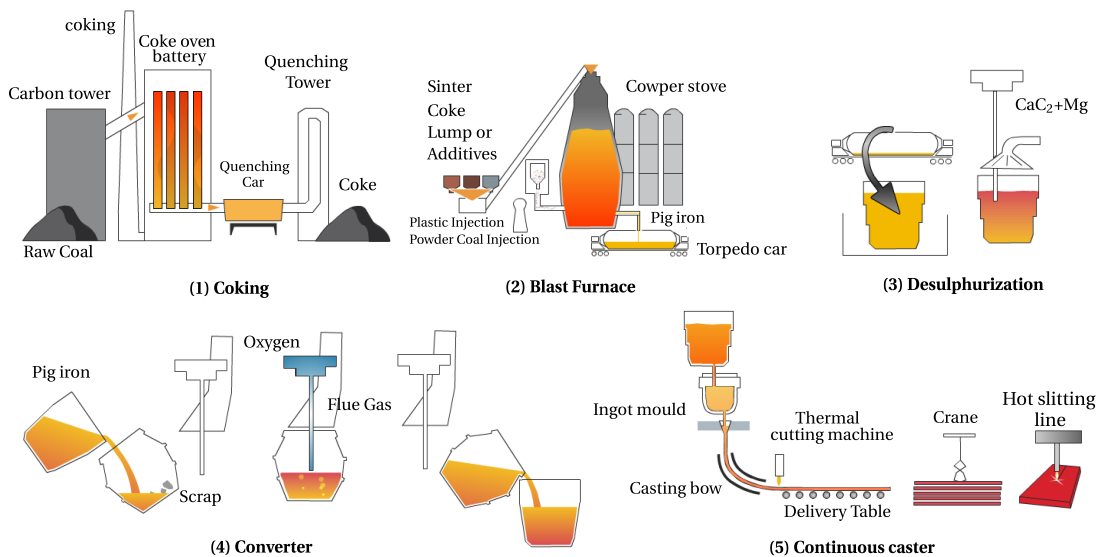


**Fig. 1.1 – Main steps in an integrated steel plant**

### Hot tearing

This defect, also denoted solidification cracking or hot cracking, occurs in the mushy zone at high solid fractions when a failure or crack appears at specific locations, the hot spots. The temperature range in which the steel is vulnerable to hot tearing is known as the brittleness temperature range (BTR). It corresponds to solid fractions greater than 90%, with the liquid phase forming a discontinuous film. Many factors can cause the failure, but the main origin is a lack of liquid feeding required to compensate for the solidification shrinkage, in the presence of thermal stresses in the mushy region. Therefore, a crack initiates then propagates in the casting, as shown in [fig. 1.2](#).



**Fig. 1.2 – Crack in an aluminium slab**

## Porosity

Porosity is a void defect formed inside the casting or at the outer surface. It may attributed to two different factors. Firstly, we speak of *shrinkage porosity*, when a void forms as a result of density differences between the interdendritic liquid and solid network, the latter being denser than the former (figs. 1.3c and 1.3d). It is basically, the same reason that initiates hot cracks. The second factor is the presence of dissolved gaseous phases in the melt (figs. 1.3a and 1.3b). According to Dantzig et al. [2009], these gases may be initially in the melt, or created by the reaction between the metal and water found in the air or trapped in grooves at the moulds surface. If the decreasing temperature and pressure drop in the liquid are large enough, the latter becomes supersaturated. Consequently, the nucleation of gaseous phase is triggered (just like when a cold bottle of coca-cola is opened !).



(a) Gas porosity in casting [AFS 2014].



(b) Shrinkage porosity [AFS 2014].



(c) Gas porosity in aluminium welding [WeldReality 2014].



(d) Xray of volume void inside welded duplex steel [ESAB 2014].

**Fig. 1.3 – Examples of porosity in casting and welding**

## Freckles or segregated channels

The origin of this defect is a combined effet of microsegregation and buoyancy forces. Upon solidification, solid forms while rejecting some solute in the liquid due to partitioning (steels have a partition coefficient less than unity). When segregated solute is the lighter species, an increasing concentration in the liquid phase produces a solutal

driving force inside the mushy zone, generating unstable convection currents, with "plume" shapes as often reported in the literature [Sarazin et al. 1992; Schneider et al. 1997; Shevchenko et al. 2013]. Temperature gradient is often an additional force of convection, the latter is hence qualified as "thermosolutal".

## 1.2 Macrosegregation

Macrosegregation generally stems from a solubility difference between a liquid phase and one or more solid phases, along with a relative velocity between these phases. While the former is responsible for local solute enrichment or depletion, the latter will propagate the composition heterogeneity on a scale much larger than just a few dendrites. This is why macrosegregation could be observed on the scale of a casting, up to several meters in length. While microsegregation can be healed by annealing the alloy to speed up the diffusion process and allow homogenization, heterogeneities spanning on larger distances cannot be treated after solidification. It is obvious that macrosegregation is irreversible defect. Failure to prevent it, may lead to a substantial decline in the alloy's mechanical behavior, hence its serviceability.

### 1.2.1 Causes

Four main factors can (simultaneously) cause fluid flow leading to macrosegregation:

#### Liquid dynamics

During solidification, thermal and solutal gradients result in density gradients in the liquid phase:

$$\rho^l = \rho_0^l(1 - \beta_T(T - T_0) - \sum_i \beta_{w_i^l}(w_i^l - \langle w_i \rangle_0^l)) \quad (1.1a)$$

$$\vec{\nabla} \rho^l = -\rho_0^l(\beta_T \vec{\nabla} T + \sum_i \beta_{w_i^l} \vec{\nabla} w_i^l) \quad (1.1b)$$

In eq. (1.1a), density is assumed to vary linearly with temperature and phase composition for each chemical species (index  $i$ ). The slopes defining such variations are respectively the thermal expansion coefficient  $\beta_T$  and the solutal expansion coefficients  $\beta_{w_i^l}$ , given by:

$$\beta_T = -\frac{1}{\rho_0^l} \left( \frac{\partial \rho^l}{\partial T} \right) \quad (1.2a)$$

$$\beta_{w_i^l} = -\frac{1}{\rho_0^l} \left( \frac{\partial \rho^l}{\partial w_i^l} \right) \quad (1.2b)$$

The linear fit assumes also that the density takes a reference value,  $\rho_0^l$ , when temperature and liquid composition reach reference values, respectively  $T_0$  and  $\langle w_i \rangle_0^l$ , while the coefficients  $\beta_{awil}$  remain constant. However, in some situations, a suitable thermodynamic database providing accurate density values is far better than a linear fit, especially in the current context of macrosegregation. Such possibility will be discussed later in the manuscript (cf. SECTION TODO)

In the presence of gravity, the density gradient in eq. (1.1b), causes thermosolutal convection in the liquid bulk and a subsequent macrosegregation.

### Solidification shrinkage

Solid alloys generally have a greater density than the liquid phase ( $\rho^s > \rho^l$ ), thus occupy less volume, with the exception of silicon where the opposite is true. Upon solidification, the liquid moves towards the solidification front to compensate for the volume difference caused by the phase change, as well as the thermal contraction. When macrosegregation is triggered by solidification shrinkage, we speak of *inverse segregation*: while one would naturally expect negative macrosegregation in areas where solidification begins and positive inside the alloy, shrinkage promotes the opposite phenomenon, by bringing solute-richer liquid towards the solidifying areas, thus raising their solute content, and resulting in a positively segregated solid. In contrast to liquid convection, shrinkage flow may cause macrosegregation even without gravity.

### Movement of equiaxed grains

Equiaxed grains can grow in the liquid bulk where thermal gradients are weak, or in the presence of inoculants. Consequently, they are transported by the flow (floating or sedimenting, depending on their density [Beckermann 2002]) which leads to negative macrosegregation in their final position.

### Solid deformation

Stresses of thermal and mechanical nature are always found in casting processes (e.g. bulging between rolls in continuous casting). Deformation of the semi-solid in the mushy zone causes a relative solid-liquid flow in the inward (tensile stresses) or outward (compressive stresses) direction, causing macrosegregation.

### 1.2.2 Examples

#### In continuous casting

The partially solidified slab is carried through a series of rolls that exert contact forces to straighten it. As the mushy part of a slab enters through these rolls, interdendritic liquid is expelled backwards, i.e. regions with lower solid fraction. Since the boundaries solidify earlier than the centre, the enriched liquid accumulates halfway in thickness, forming a centreline macrosegregation as shown in [fig. 1.4](#). Other types of segregates (channels, A-segregates ...) can also be found but remain more specific to ingot casting.

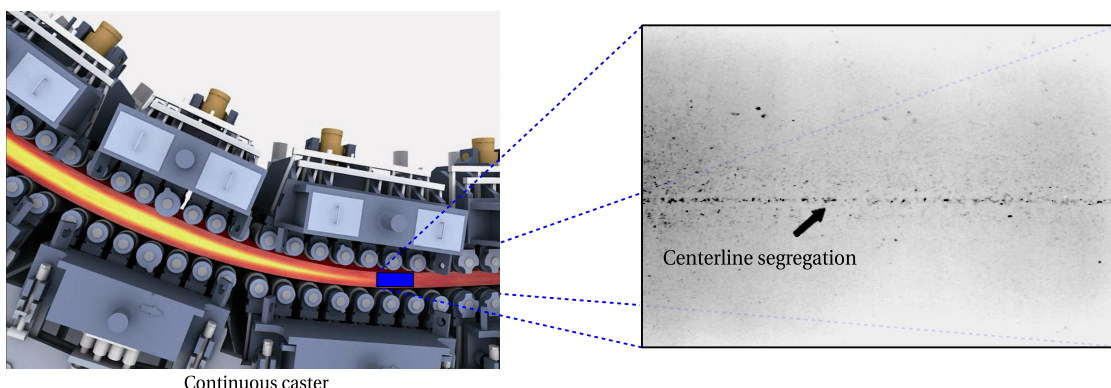


**Fig. 1.4 – Centreline segregation in a steel slab [Beckermann 2002]**

#### In ingot casting

A variety of segregation patterns can be encountered in heavy ingots:

- the lower part is characterized by a negative segregation cone promoted by the sedimentation of equiaxed crystals,
- positive segregation channels, known as A-segregates, form along the columnar dendritic zones, close to the vertical contact with the mould,
- positive V-segregates can be identified in the centre of the ingot,
- a positive macrosegregation in the upper zone where the last liquid solidifies, the so-called "hot-top", caused by solidification shrinkage (inverse segregation) and thermosolutal buoyancy forces.

[Combeau et al. \[2009\]](#) state that A-segregates and V-segregates formation is mainly attributed to local flow phenomena. As such, their scale is finer than macrosegregation, hence called "mesosegregates".

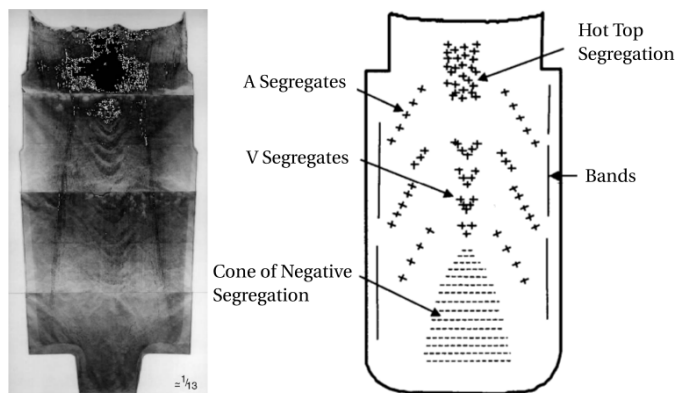
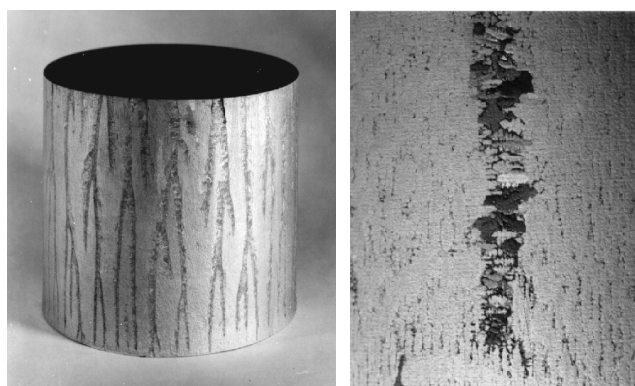


**Fig. 1.5** – Sulphur print (left) of a 65-ton steel ingot [Lesoult 2005] showing various patterns (right) of macrosegregation [Flemings 1974]

### In investment casting

This process is widely used to cast single-crystal (SC) alloys for turbines and other applications that require excellent mechanical behavior [Giamei et al. 1970]. When performed by directional solidification, thermosolutal forces thrust segregated species outside of the mushy zone into the liquid bulk. The segregation scale ranges from a few dendrites to a few hundreds of them, hence forming "long and narrow trails" (fig. 1.6a) as described by Felicelli et al. [1991]. Freckles are frequently formed by small equiaxed grains (fig. 1.6b), probably caused by a uniform temperature gradient that settles as the channels become richer in solute. They can be observed on the ingot's surface, as well as in the volume.



(a) Small cylinder ingot showing freckles on the outer surface  
 (b) Zoomed image showing the microstructure in one freckle

**Fig. 1.6** – Freckles in directional casting of nickel-base superalloys

### 1.3 Industrial Worries

**Steel production** has continuously increased over the years to meet the industrial needs. [Figure 1.7](#) shows this increase between 1980 and 2013 with a clear dominance of the Chinese production. Quality constraints have also increased where specific grades of steel are needed in critical applications such as mega-structures in construction and heavy machinery. Therefore, alloys with defects are considered vulnerable and should be avoided as much as possible during the casting process. As such, steelmakers have been investing in research, with the aim of understanding better the phenomena leading to casting problems, and improve the processes when possible.

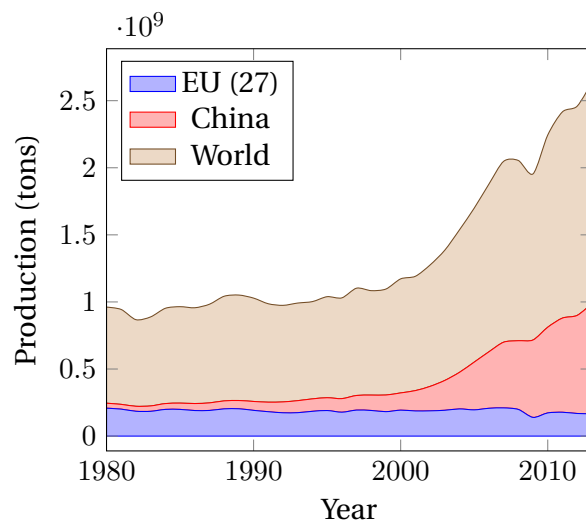


**Fig. 1.7** – Evolution curves of crude steel worldwide production from 1980 to 2013 [[WSA 2014](#)].

**Simulation software** dedicated to alloy casting is one of the main research investments undertaken by steelmakers. These tools coming from academic research are actively used to optimize the process. However, few are the tools that take into account the casting environment. For instance, the continuous casting process, in [fig. 1.1](#), is a chain process where the last steps involve rolls, water sprays and other components. A dedicated software is one that can provide the geometric requirements with suitable meshing capabilities, as well as respond to metallurgical and mechanical requirements, mainly:

- handling moulds and their interaction with the alloy (thermal resistances ...)
- handling alloy filling and predicting velocity in the liquid and mushy zone
- handling thermomechanical stresses in the solid
- handling multicomponent alloys and predicting macrosegregation
- handling finite solute diffusion in solid phases

- handling real alloy properties (not just constant thermophysical/thermomechanical properties)

## **1.4 Project context and objectives**

### **1.4.1 Context**

The European Space Agency (ESA) has been actively committed, since its foundation in 1975, in the research field. Its covers not only exclusive space applications, but also fundamental science like solidification. This thesis takes part of the ESA project entitled *CCEMLCC*, abbreviating "Chill Cooling for the Electro-Magnetic Levitator in relation with Continuous Casting of steel". The three-year contract from 2011 to late 2014 denoted *CCEMLCC II*, was preceded by an initial project phase, *CCEMLCC I*, from 2007 to 2009. The main focus is studying containerless solidification of steel under microgravity conditions. A chill plate is later used to extract heat from the alloy, simulating the contact effect with a mould in continuous casting or ingot casting. A partnership of 7 industrial and academic entities was formed in *CCEMLCC II*. Here is a brief summary of each partner's commitment:

#### **Academic partners**

- Center for Material Forming (CEMEF) - France: numerical modelling of microgravity chill cooling experiments
- Deutsches Zentrum für Luft- und Raumfahrt (DLR or German Aerospace Centre) and Ruhr Universität Bochum (RUB) university - Germany: preparation of a chill cooling device for electromagnetic levitation (EML), microgravity testing and investigation of growth kinetics in chill-cooled and undercooled steel alloys
- University of Alberta - Canada: impulse atomization of the D2 tool steel
- University of Bremen - Institut für Werkstofftechnik (IWT) institute - Germany: study of melt solidification in spray forming and atomization processing

#### **Industrial partners**

- ARCELORMITTAL (France): elaboration of a series of steel grades used in microgravity and ground studies
- METSO Minerals Inc. (Finland): material production with D2 tool steel for spray forming
- TRANSVALOR (France): development and marketing of casting simulation software *Thercast*®

CEMEF, as an academic partner, contributed to the work by proposing numerical models in view of predicting the chill cooling of steel droplets. A first model was developed by [Rivaux \[2011\]](#) whereas the present thesis discusses a new model. The experimental work considered various facilities and environments to set a droplet of molten alloy in levitation: EML ([fig. 1.8](#)) for ground-based experiments, microgravity in parabolic flight or sounding rockets and last, microgravity condition on-board the International Space Station (ISS)

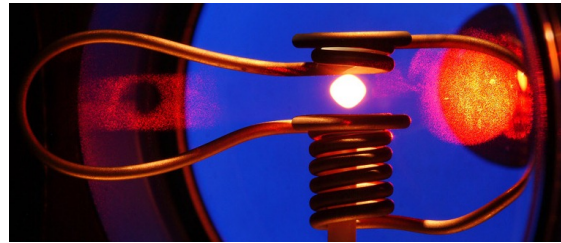


**Fig. 1.8 – Electromagnetic levitation [DLR 2014].**

### 1.4.2 Objectives and outline

The main focus of the present thesis is predicting macrosegregation with liquid dynamics assuming a fixed solid phase, i.e. no account of solid transport (e.g. equiaxed crystals sedimentation) and no account of solid deformation. In CEMEF, this scope has been adopted for previous work by [Gouttebroze \[2005\]](#), [Liu \[2005\]](#), [Mosbah \[2008\]](#), [Rivaux \[2011\]](#), and [Carozzani \[2012\]](#). Nevertheless, many modelling features evolved with time such as going from two-dimensional to three-dimensional modelling, resolution schemes for each of the conservation equations: energy, chemical species and liquid momentum, Eulerian or Lagrangian descriptions, modelling of grain structure and others. In this thesis, we propose a numerical model that takes into account i) the energy conservation in a temperature formulation based on a thermodynamic database mapping, ii) the liquid momentum conservation with thermosolutal convection and solidification shrinkage as driving forces, iii) solute mass conservation and iv) solidification paths at full equilibrium for multicomponent alloys microsegregation. Moreover, all equations are formulated in a pure Eulerian description while using the Level Set method to keep implicitly track of the interface between the alloy and surrounding gas. To the author's knowledge, this work combining macrosegregation prediction using the level set methodology to track the metal-air interface during shrinkage has no precedent in casting and solidification literature. The model couples in a weak fashion, all four conservation equations presented in [fig. 1.9](#), showing on the one hand, that microsegregation is an essential common link between these equations, while on the other hand, the level set interacts with conservations equations by giving the interface position.

## 1.4. Project context and objectives

---

Numerical tools: Cimlib relying on PETSc, parallelised with MPICH2, paraview and python as tools for postprocess and analysis.

The previously mentionned simulation requirements are not met in a single casting software package. Nevertheless, *Thercast<sup>®</sup>* is a promising tool that already handles a part of the above points. The current thesis developments are done using C++ language as a part of the in-house code, known as *CimLib* [Digonnet et al. 2007; Mesri et al. 2009]. This fully parallel library is the main academic research support for *Thercast<sup>®</sup>*.

Outline: each chapter content ...

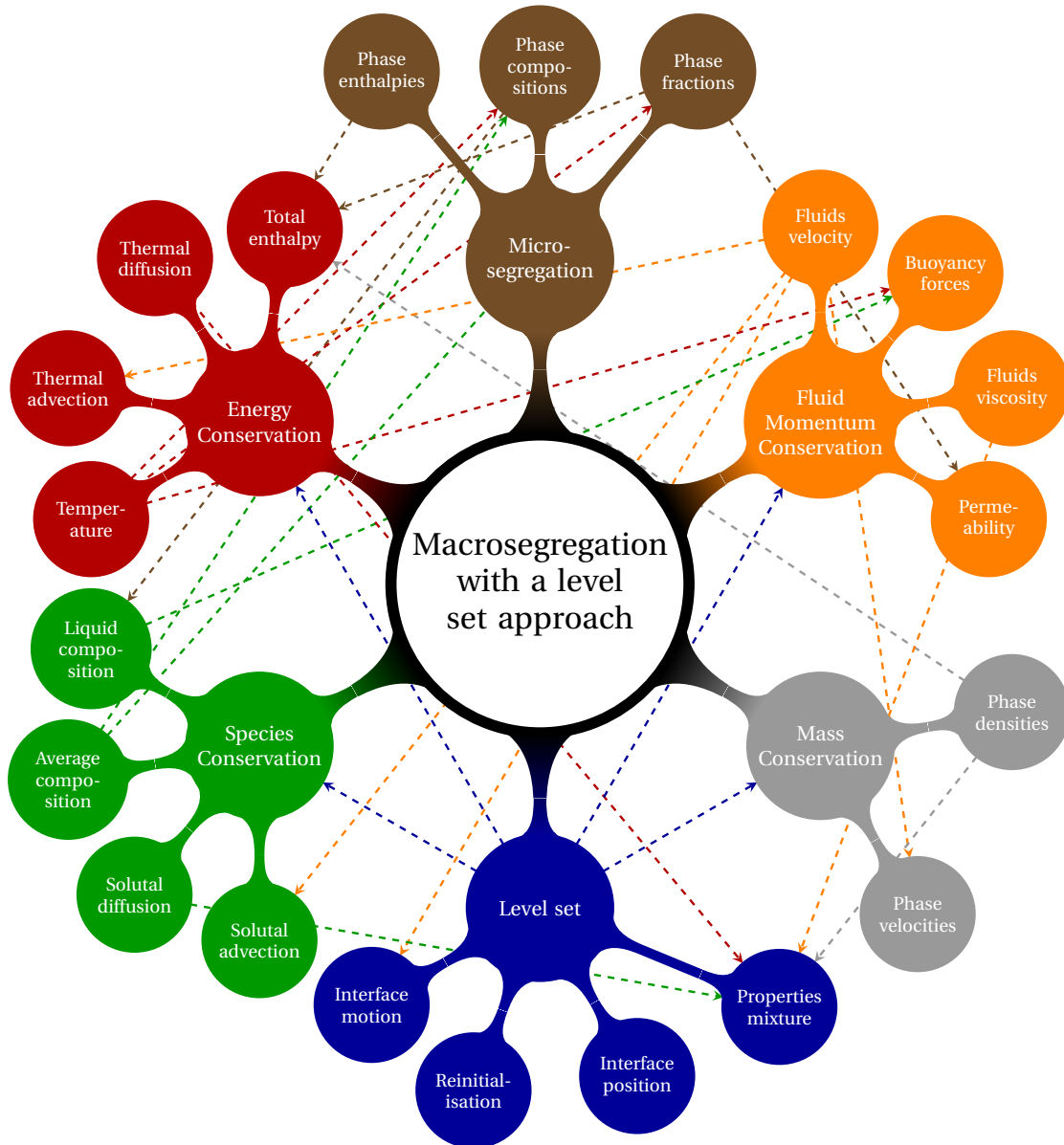


**Fig. 1.9** – A graphical representation of the main ingredients of the numerical approach, for a macrosegregation model with the level set methodology, when no solid deformation or movement are considered. The dashed lines represent the possible interaction between the components.

# Chapter 5

## Macrosegregation with solidification shrinkage

### Contents

---

<b>5.1</b>	<b>Introduction</b>	<b>92</b>
<b>5.2</b>	<b>FE model: Metal</b>	<b>92</b>
5.2.1	Mass and momentum conservation	94
5.2.2	Energy conservation	95
5.2.3	Species conservation	97
<b>5.3</b>	<b>FE model: Air</b>	<b>99</b>
5.3.1	Mass and momentum conservation	100
5.3.2	Energy conservation	100
5.3.3	Species conservation	100
<b>5.4</b>	<b>FE monolithic model</b>	<b>100</b>
5.4.1	Permeability mixing	100
5.4.2	Model equations	101
5.4.3	Interface treatment	101
<b>5.5</b>	<b>Shrinkage without macrosegregation</b>	<b>103</b>
5.5.1	Al-7wt% Si	104
5.5.2	Pb-3wt% Sn	104
<b>5.6</b>	<b>Shrinkage with macrosegregation</b>	<b>104</b>
5.6.1	Al-7wt% Si	104
5.6.2	Pb-3wt% Sn	104

---

## 5.1 Introduction

Solidification shrinkage is, by definition, the effect of relative density change between the liquid and solid phases. In general, it results in a progressive volume change during solidification, until the phase change has finished. The four stages in [figs. 5.1a](#) to [5.1d](#) depict the volume change with respect to solidification time. First, at the level of the first solid crust, near the local solidus temperature, the solid forms with a density smaller than the liquid's. This does not necessarily apply for all materials, but at least for steels it does. The subsequent volume difference tends to create voids with a big negative pressure, that needs to be compensated by a surrounding fluid. It thus drains the liquid metal in its direction (cf. [Figure 5.1b](#)). As a direct result of the inward feeding flow, the ingot surface tends to gradually deform in the feeding direction, forming the so-called *shrinkage pipe*. Since the mass of the alloy and its chemical species is conserved, a density difference between the phases ( $\rho^l < \rho^s \implies \frac{\rho^l}{\rho^s} < 1$ ) eventually leads to a different overall volume ( $V^s < V^l$ ) once solidification is complete, as confirm the following equations:

$$\rho^l V^l = \rho^s V^s \quad (5.1a)$$

$$V^s = \frac{\rho^l}{\rho^s} V^l \quad (5.1b)$$

Solidification shrinkage is not the only factor responsible for volume decrease. Thermal shrinkage in both solid and liquid phases, as well as solutal shrinkage in the liquid phase are also common causes in a casting process. Henceforth, we will focus on shrinkage due to phase change.

### Literature review

Talk and explain models in the literature that predict shrinkage (without or with macrosegregation): Beckermann, Wu ?

Show and comment the experiments that have been done: Hebditch and Hunt, Smacs Hachani ...

**Sutaria2012** talk about feeding paths, but more importantly they computed thermal shrinkage WITHOUT solving NavierStokes equations. To predict the interface shape, they solve a LS transport with an imposed velocity given by Gada et Sharma 2009

## 5.2 FE model: Metal

In this section, we start from a the monodomain finite element model presented in [section 2.1.4](#) relevant to metal only, then present the essential assumptions and formulations that allow predicting solidification shrinkage in a Eulerian context.

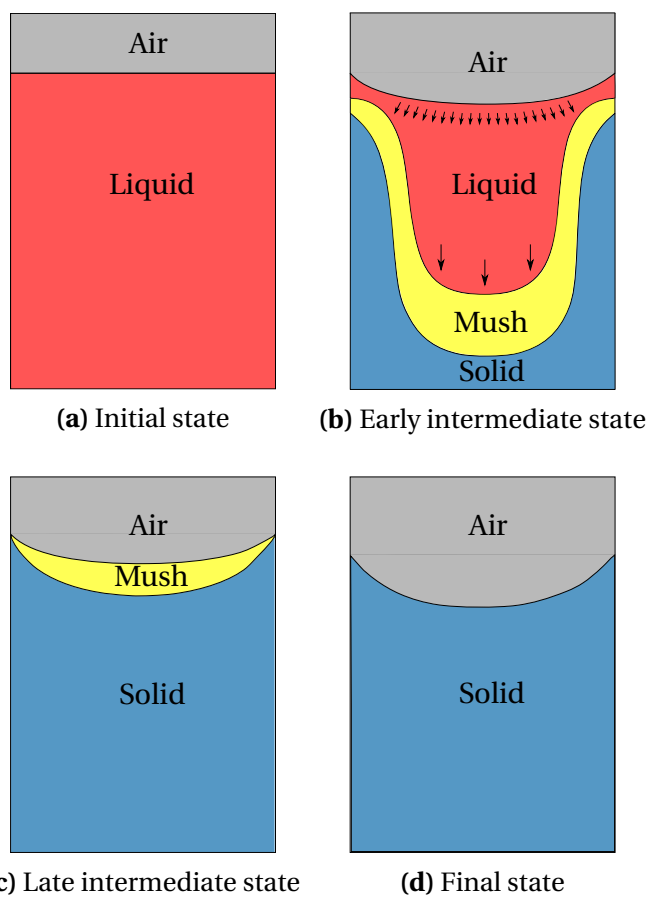


**Fig. 5.1** – Schematic of the main cooling stages of an ingot against side and bottom mould walls (not shown)

### 5.2.1 Mass and momentum conservation

#### Assumptions

- Two phases are considered, liquid  $l$  and solid  $s$ :  $g^l + g^s = 1$
- The phase densities are constant but not equal:  $\rho^l = cst_1$  and  $\rho^s = cst_2$ . Thermal and solutal expansion/contraction is neglected
- The solid phase is assumed static:  $\vec{v}^s = \vec{0}$ , which yields the following consequences:
  1.  $\langle \vec{v} \rangle = g^l \vec{v}^l + g^s \vec{v}^s = g^l \vec{v}^l$
  2.  $\langle \rho \vec{v} \rangle = g^l \rho^l \vec{v}^l + g^s \rho^s \vec{v}^s = g^l \rho^l \vec{v}^l$
  3.  $\vec{\nabla} \rho^l = \vec{\nabla} \rho^s = \vec{0}$

#### Formulation

The mass balance equation averaged over the two phases, is expanded taking into account the aforementioned assumptions.

$$\frac{\partial \langle \rho \rangle}{\partial t} + \nabla \cdot \langle \rho \vec{v} \rangle = 0 \quad (5.2a)$$

$$\frac{\partial}{\partial t} (g^l \rho^l + g^s \rho^s) + \nabla \cdot (g^l \rho^l \vec{v}^l) = 0 \quad (5.2b)$$

$$g^l \frac{\partial \rho^l}{\partial t} + \rho^l \frac{\partial g^l}{\partial t} + g^s \frac{\partial \rho^s}{\partial t} + \rho^s \frac{\partial g^s}{\partial t} + \rho^l \nabla \cdot (g^l \vec{v}^l) + g^l \vec{v}^l \cdot \vec{\nabla} \rho^l = 0 \quad (5.2c)$$

$$(\rho^l - \rho^s) \frac{\partial g^l}{\partial t} + \rho^l \nabla \cdot (g^l \vec{v}^l) = 0 \quad (5.2d)$$

$$\nabla \cdot (g^l \vec{v}^l) = \nabla \cdot \langle \vec{v}^l \rangle = \frac{\rho^l - \rho^s}{\rho^l} \frac{\partial g^s}{\partial t}$$

(5.3)

With the assumptions of static solid phase and constant unequal phase densities, the average mass balance states that the divergence of the liquid velocity is proportional to the solidification rate, by a factor of density change, which results in a relative volume change. [Equation \(5.3\)](#) explains the flow due to shrinkage. In metallic alloys, the solid density is usually greater than the liquid density, therefore the first term in the RHS is negative. As for the second term, if we neglect remelting, then it'll be positive in the solidifying areas of the alloy. A negative divergence term in these areas, means that a liquid feeding is necessary to compensate for the density difference, hence acting as a flow driving force in the melt. In the case of constant densities, we can easily deduce that the divergence term is null, and therefore no flow is induced by solidification. Furthermore, additional terms should appear in the other conservation equations, bal-

ancing the volume change in the heat and species transport. When the metal's density was considered constant during solidification, the assumption of an incompressible system made it possible to use the Boussinesq approximation. However, in the case of solidification shrinkage, the average density  $\langle \rho \rangle = g^s \rho^s + g^l \rho^l$  varies, since  $\rho^s$  and  $\rho^l$  are not equal. Naturally, these phase densities would depend on temperature and possibly on the phase composition. Therefore, the incrompressibility condition may not be true. In such case, the earlier given system eq. (2.44) is reformulated without any reference value for density:

$$\left\{ \begin{array}{l} \rho^l \left( \frac{\partial \langle \vec{v}^l \rangle}{\partial t} + \frac{1}{g^l} \vec{\nabla} \cdot (\langle \vec{v}^l \rangle \times \langle \vec{v}^l \rangle) \right) = \\ - g^l \vec{\nabla} p^l - 2\mu^l \vec{\nabla} \cdot (\overline{\nabla} \langle \vec{v}^l \rangle + \overline{\nabla}^t \langle \vec{v}^l \rangle) - g^l \mu^l \mathbb{K}^{-1} \langle \vec{v}^l \rangle + g^l \rho^l \vec{g} \\ \nabla \cdot \langle \vec{v}^l \rangle = \frac{\rho^l - \rho^s}{\rho^l} \frac{\partial g^s}{\partial t} \end{array} \right. \quad (5.4)$$

### 5.2.2 Energy conservation

We have seen the averaged energy conservation equation in the case of two phases: a solid phase and an incompressible liquid phase. However, with the incorporation of the shrinkage effect, new terms should appear in the advective-diffusive heat transfer equation.

#### Assumptions

- The thermal conductivity is constant for both phases:  $\langle \kappa \rangle = \langle \kappa^s \rangle = \langle \kappa^l \rangle = \kappa$
- Consequence of the static solid phase:  $\langle \rho h \vec{v} \rangle = g^l \rho^l h^l \vec{v}^l + g^s \rho^s h^s \vec{v}^s = g^l \rho^l h^l \vec{v}^l$
- The system's enthalpy may thermodynamically evolve with pressure, knowing that  $h = e + \frac{p}{\rho}$ , where  $e$  is the internal energy and  $p$  is the pressure. It infers that the heat transport equation may contain a contribution attributed to volume compression/expansion:

$$\frac{\partial p}{\partial t} + \nabla \cdot (p \vec{v}) = \frac{\partial p}{\partial t} + p \nabla \cdot \vec{v} + \vec{v} \cdot \vec{\nabla} p \quad (5.5)$$

In the literature, this contribution has been always neglected, even when accounting for solidification shrinkage, owing to the small variations of pressure.

- The heat generated by mechanical deformation,  $\mathbb{S} : \dot{\varepsilon}$ , is neglected

## Formulation

The unknowns in the energy conservation are the average volumetric enthalpy  $\langle \rho h \rangle$  and temperature  $T$ . The energy conservation equation writes:

$$\frac{\partial \langle \rho h \rangle}{\partial t} + \nabla \cdot (\langle \rho h \vec{v} \rangle) = \nabla \cdot (\langle \kappa \vec{\nabla} T \rangle) \quad (5.6a)$$

$$\frac{\partial \langle \rho h \rangle}{\partial t} + \nabla \cdot (g^l \rho^l h^l \vec{v}^l) = \nabla \cdot (\kappa \vec{\nabla} T) \quad (5.6b)$$

$$\frac{\partial \langle \rho h \rangle}{\partial t} + \rho^l h^l \nabla \cdot \langle \vec{v}^l \rangle + \langle \vec{v}^l \rangle \cdot \vec{\nabla} (\rho^l h^l) = \nabla \cdot (\kappa \vec{\nabla} T) \quad (5.6c)$$

$$\frac{\partial \langle \rho h \rangle}{\partial t} + \rho' h^l \frac{\rho^l - \rho^s}{\rho'} \frac{\partial g^s}{\partial t} + \langle \vec{v}^l \rangle \cdot \vec{\nabla} (\rho^l h^l) = \nabla \cdot (\kappa \vec{\nabla} T) \quad (5.6d)$$

$$\frac{\partial \langle \rho h \rangle}{\partial t} + (\rho^l - \rho^s) h^l \frac{\partial g^s}{\partial t} + \langle \vec{v}^l \rangle \cdot \vec{\nabla} (\rho^l h^l) = \nabla \cdot (\kappa \vec{\nabla} T) \quad (5.6e)$$

$$\frac{\partial \langle \rho h \rangle}{\partial t} + \rho^l \langle \vec{v}^l \rangle \cdot \vec{\nabla} h^l = \nabla \cdot (\kappa \vec{\nabla} T) + (\rho^s - \rho^l) h^l \frac{\partial g^s}{\partial t} \quad (5.7)$$

In order to keep things simple, the term "enthalpy" will refer henceforth to "volume enthalpy", otherwise, we will explicitly use the term "mass enthalpy". It is important to understand the meaning of the terms in equation (5.7). The first term in the left-hand side is the temporal change in the system's average enthalpy, i.e. a temporal change in the volume enthalpy of any of the phases in the course of solidification. The second LHS term is a dot product between the superficial liquid velocity and the gradient of the liquid's enthalpy. Since phase densities are constant in our case, the gradient term reduces to the liquid's mass enthalpy. If we consider a representative volume element (RVE) in the liquid phase, far from the mushy zone, we can stipulate:

$$\vec{\nabla} h^l = C_p^l \vec{\nabla} T \quad (5.8)$$

assuming that the phase mass specific heat,  $C_p^l$ , is constant. Therefore, the liquid enthalpy is advected in the case where the velocity vector is not orthogonal to the temperature gradient. The advection reaches its maximum when the two vectors have the same direction. Consider, for instance, a filled ingot with a cooling flux applied to its bottom surface. If the density variation with temperature were to be neglected, then the sole mechanical driving force in the melt is the density jump at the solid-liquid interface ahead of the mushy zone. The temperature gradient in such a case is vertical upward, while the velocity vector is in the opposite direction. The advective term writes:

$$\rho^l \langle \vec{v}^l \rangle \cdot \vec{\nabla} h^l = -\rho^l C_p^l \|\langle \vec{v}^l \rangle\| \|\vec{\nabla} T\| \quad (5.9)$$

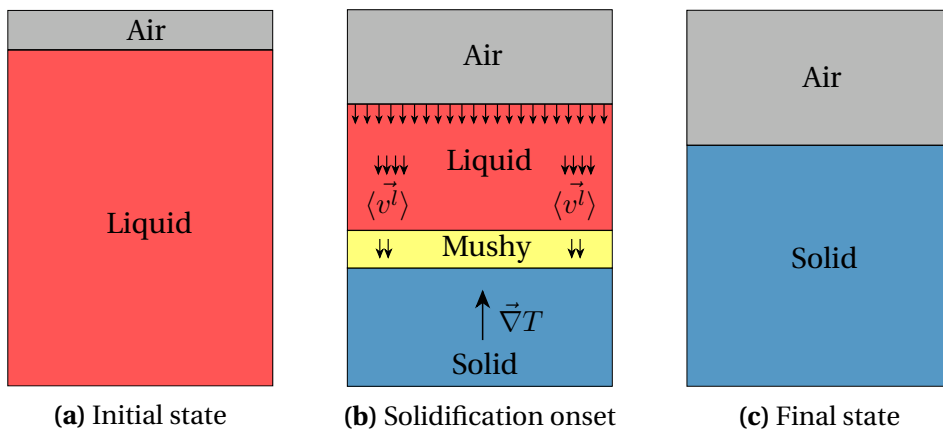


**Fig. 5.2 – Effect of one-dimensional shrinkage flow on a solidifying ingot**

We see that the second LHS term in equation (5.7) acts as a heat source at the interface between the phases, in this particular solidification scenario. Another heat power (of unit  $Wm^{-3}$ ) adds to the system in the mushy zone, that is the second term in the RHS of the same equation. This term is proportional to the solidification rate. Finally, the first RHS term accounts for thermal diffusion within the phases.

It should be emphasized that the assumption of a constant specific heat in the liquid in equation (5.8) applies when no macrosegregation occurs. Nonetheless, when the latter is considered, the phases specific and latent heats become highly dependent on the local average composition. It then advisable to use the thermodynamic tabulation approach, where the enthalpies are directly tabulated as functions of temperature and intrinsic phase compositions.

### 5.2.3 Species conservation

The last conservation principle is applied to the chemical species or solutes. This principle allows predicting macrosegregation when applied to a solidification system, along with the mass, momentum and energy balances. However, the conservation equation should be reformulated in the case of a melt flow driven by shrinkage.

#### Assumptions

- The alloy is binary, i.e. it is composed from one solute, and hence the notation of the average composition without a solute index:  $\langle w \rangle$  for the mass composition and  $\langle \rho w \rangle$  for the volume composition
- The solid fraction is determined assuming complete mixing in both phases, hence the lever rule is applied. The solidification path in the current approach is tabulated using thermodynamic data at equilibrium

## Chapter 5. Macrosegregation with solidification shrinkage

---

- The macroscopic solute diffusion coefficient  $D^s$  in the solid phase is neglected in the mass diffusive flux term.
- The solid phase is fixed and rigid, therefore  $\langle \rho w \vec{v} \rangle = g^l \rho^l \langle w \rangle^l \vec{v}^l + g^s \rho^s \langle w \rangle^s \vec{v}^s = g^l \rho^l \langle w \rangle^l \vec{v}^l$

### Formulation

The species conservation is pretty similar the energy conservation formulated in the previous section. For a binary alloy, we write:

$$\frac{\partial \langle \rho w \rangle}{\partial t} + \nabla \cdot \langle \rho w \vec{v} \rangle - \nabla \cdot \left( \langle D^l \rangle \vec{\nabla} (\rho^l \langle w \rangle^l) \right) = 0 \quad (5.10a)$$

$$\langle \rho \rangle \frac{\partial \langle w \rangle}{\partial t} + \langle w \rangle \frac{\partial \langle \rho \rangle}{\partial t} + \nabla \cdot \left( g^l \rho^l \langle w \rangle^l \vec{v}^l \right) - \nabla \cdot \left( g^l D^l \vec{\nabla} (\rho^l \langle w \rangle^l) \right) = 0 \quad (5.10b)$$

$$\begin{aligned} \langle \rho \rangle \frac{\partial \langle w \rangle}{\partial t} + \langle w \rangle \frac{\partial \langle \rho \rangle}{\partial t} &+ \left( \rho^l \langle w \rangle^l \right) \nabla \cdot \langle \vec{v}^l \rangle + \langle \vec{v}^l \rangle \cdot \vec{\nabla} (\rho^l \langle w \rangle^l) \\ &- \nabla \cdot \left( g^l D^l \vec{\nabla} (\rho^l \langle w \rangle^l) \right) = 0 \end{aligned} \quad (5.10c)$$

The mass balance gives the following relations:

$$\frac{\partial \langle \rho \rangle}{\partial t} + \nabla \cdot \langle \rho \vec{v} \rangle = 0 \quad (5.11a)$$

$$\frac{\partial \langle \rho \rangle}{\partial t} + \nabla \cdot \left( g^l \rho^l \vec{v}^l \right) = 0 \quad (\rho^l \text{ is constant}) \quad (5.11b)$$

$$\nabla \cdot \langle \vec{v}^l \rangle = -\frac{1}{\rho^l} \frac{\partial \langle \rho \rangle}{\partial t} \quad (5.11c)$$

If we use the result of eq. (5.11c) in eq. (5.10c), then we get the following equation:

$$\langle \rho \rangle \frac{\partial \langle w \rangle}{\partial t} + \langle w \rangle \frac{\partial \langle \rho \rangle}{\partial t} = \langle w \rangle^l \frac{\partial \langle \rho \rangle}{\partial t} - \langle \vec{v}^l \rangle \cdot \vec{\nabla} (\rho^l \langle w \rangle^l) + \nabla \cdot \left( g^l D^l \vec{\nabla} (\rho^l \langle w \rangle^l) \right) \quad (5.12)$$

Applying Voller-Prakash [Voller et al. 1989] variable splitting, the system ends up with only one variable, which is the average composition  $\langle w \rangle$ . The splitting is done as follows:

$$\langle w \rangle^l = \left( \langle w \rangle^l \right)^t + \langle w \rangle - \langle w \rangle^t \quad (5.13)$$

where the superscript  $t$  refers to the previous time step. The chemical species conservation writes:

$$\begin{aligned} \langle \rho \rangle \frac{\partial \langle w \rangle}{\partial t} + \cancel{\langle w \rangle} \frac{\partial \langle \rho \rangle}{\partial t} = \\ \cancel{\langle w \rangle} \frac{\partial \langle \rho \rangle}{\partial t} - \rho^l \langle \vec{v}^l \rangle \cdot \vec{\nabla} \langle w \rangle + \nabla \cdot \left( g^l \rho^l D^l \nabla \langle w \rangle \right) \\ + \frac{\partial \langle \rho \rangle}{\partial t} \left[ \left( \langle w \rangle^l \right)^t - \langle w \rangle^t \right] - \rho^l \langle \vec{v}^l \rangle \cdot \vec{\nabla} \left( \langle w \rangle^t - \left( \langle w \rangle^l \right)^t \right) \end{aligned} \quad (5.14a)$$

$$\begin{aligned} \langle \rho \rangle \frac{\partial \langle w \rangle}{\partial t} + \rho^l \langle \vec{v}^l \rangle \cdot \vec{\nabla} \langle w \rangle - \nabla \cdot \left( g^l \rho^l D^l \nabla \langle w \rangle \right) = \\ - \frac{\partial \langle \rho \rangle}{\partial t} \left[ \langle w \rangle^t - \left( \langle w \rangle^l \right)^t \right] + \rho^l \langle \vec{v}^l \rangle \cdot \vec{\nabla} \left( \langle w \rangle^t - \left( \langle w \rangle^l \right)^t \right) \\ - \nabla \cdot \left[ g^l \rho^l D^l \vec{\nabla} \left( \langle w \rangle^t - \left( \langle w \rangle^l \right)^t \right) \right] \end{aligned} \quad (5.14b)$$

$$\begin{aligned} \langle \rho \rangle \frac{\partial \langle w \rangle}{\partial t} + \rho^l \langle \vec{v}^l \rangle \cdot \vec{\nabla} \langle w \rangle - \nabla \cdot \left( g^l \rho^l D^l \nabla \langle w \rangle \right) = \\ - \frac{\partial \langle \rho \rangle}{\partial t} \left[ \langle w \rangle^t - \left( \langle w \rangle^l \right)^t \right] \\ + \rho^l \langle \vec{v}^l \rangle \cdot \vec{\nabla} \left( \langle w \rangle^t - \left( \langle w \rangle^l \right)^t \right) - \nabla \cdot \left[ g^l \rho^l D^l \vec{\nabla} \left( \langle w \rangle^t - \left( \langle w \rangle^l \right)^t \right) \right] \end{aligned} \quad (5.15)$$

It is noted that eq. (5.15) is valid only if both densities  $\rho^l$  and  $\rho^s$  are constant but have different values. Since density changes are incorporated in this equation, inverse segregation following solidification shrinkage is predicted. For the case where macrosegregation is solely due to fluid flow generated by natural or forced convection, i.e. no shrinkage occurs whether due to thermal-solutal contraction or phase change, the overall volume remains constant, hence density is constant. In this situation,  $\rho^s = \rho^l = \langle \rho \rangle$  and the term  $\partial \langle \rho \rangle / \partial t$  therefore vanishes. After dividing both sides by  $\langle \rho \rangle = \rho^l$ , eq. (5.15) reduces to:

$$\begin{aligned} \frac{\partial \langle w \rangle}{\partial t} + \langle \vec{v}^l \rangle \cdot \vec{\nabla} \langle w \rangle - \nabla \cdot \left( g^l D^l \nabla \langle w \rangle \right) \\ = \langle \vec{v}^l \rangle \cdot \vec{\nabla} \left( \langle w \rangle^t - \left( \langle w \rangle^l \right)^t \right) - \nabla \cdot \left[ g^l D^l \vec{\nabla} \left( \langle w \rangle^t - \left( \langle w \rangle^l \right)^t \right) \right] \end{aligned} \quad (5.16)$$

### 5.3 FE model: Air

Conservation equations for the air are close to those derived for the metal as a fluid, with the exception of some points:

- air is a fluid that will not undergo any phase change, hence constant heat diffusivity;
- species conservation is irrelevant in the air as it is considered a pure material;
- unlike metal, air is considered incompressible at any time.

### 5.3.1 Mass and momentum conservation

### 5.3.2 Energy conservation

### 5.3.3 Species conservation

The composition of alloying elements is crucial quantity to predict in this work. Nevertheless, such prediction is only relevant in the metallic alloy, even if the air is also made up of other chemical species (nitrogen, oxygen ...). For this obvious reason, the species conservation equation should not be solved in the air, but that of course is contradictory to the monolithic resolution. The consequence is that we should compute the conservation of chemical species in the air and the metal, but limit as much as possible the influence of the former, in a way to prevent a "numerical" solute exchange between these domains. To do so, the computed air velocity will not be used here for advection, but rather use a zero-velocity vector instead. As diffusion is also another transport mechanism that may alter the conservation principle, a very low macroscopic solute diffusion coefficient can be used, as long as its order of magnitude is at most a thousand times less than that in the melt,  $D^A \ll D^l$ . The low artificial diffusion in the air may slightly violate the wanted no-exchange condition at the air-liquid interface, but it is known that suppressing the diffusion term in the air would result in a stiff partial differential equation that may be difficult to solve.

$$\frac{\partial}{\partial t} (\rho^A \langle w \rangle^A) + \nabla \cdot \left( \rho^A \langle w \rangle^A \vec{v}^A \right) - \nabla \cdot \left( \rho^A D^A \vec{\nabla} \langle w \rangle^A \right) = 0 \quad (5.17)$$

$$\boxed{\frac{\partial}{\partial t} (\rho^A \langle w \rangle^A) - \nabla \cdot \left( \rho^A D^A \vec{\nabla} \langle w \rangle^A \right) = 0} \quad (5.18)$$

## 5.4 FE monolithic model

The monolithic model combines all conservations equations in metal and air in a unique set of equations to be solved on a fixed mesh. This can be accomplished by using the Heaviside function (defined in [section 2.4.1](#)) relative to each domain.

### 5.4.1 Permeability mixing

How to mix liquid fraction, best using harmonic or arithmetic, in order to replicate the effect the of non slip condition at top for example

Put the python plots from the presentations in "TEXUS monolithic"  
Put video animations of PSEUDO SMACS 2D without and with LS ???

### 5.4.2 Model equations

Rewrite air-metal monolithic conservation equations using mixture laws.

### 5.4.3 Interface treatment

The level set method, like any other interface tracking/capturing method, needs defining a convenient way of coupling the velocity field on the one hand, which is the solution provided by solving momentum conservation equations, with the interface position on the other hand. The question is "how does the velocity field transport the interface?". The answer is potentially one of two possibilities: classical coupling or modified coupling. In the next subsections, we discuss the technical details of each approach and the hurdles that come with it.

#### Classical coupling

A "classical" coupling comes in the sense of "unmodified" coupling. This approach consists of taking the output of the fluid mechanics solver, then feed it as raw input to level set transport solver. The physical translation would be that the interface motion is dictated by the fluids flow in its vicinity. No treatment whatsoever is done between the two mentioned steps. While conservation principles are best satisfied with this approach, the latter yields some drawbacks, preventing its application in a generic way. For instance, the free liquid surface is not necessarily horizontal at all times and that can lead to the wrong shrinkage profile when solidification is complete.

present the example of unstable interface when the ratio between fluids properties became greater than some value+discussion

#### Modified coupling

In contrast to a classic coupling, here we attempt to modify the velocity field before feeding to the transport solver. The main motivation for considering this approach is the lack of stability that we observed whenever the mechanical properties of the fluids were different by several orders of magnitude. The algorithm should simultaneously fulfil these requirements:

- support high ratios of fluids density with close viscosities by preserving an non-oscillating interface,
- maintain a horizontal level at the free surface of the melt,
- follow shrinking metal surface profile in solidifying regions,

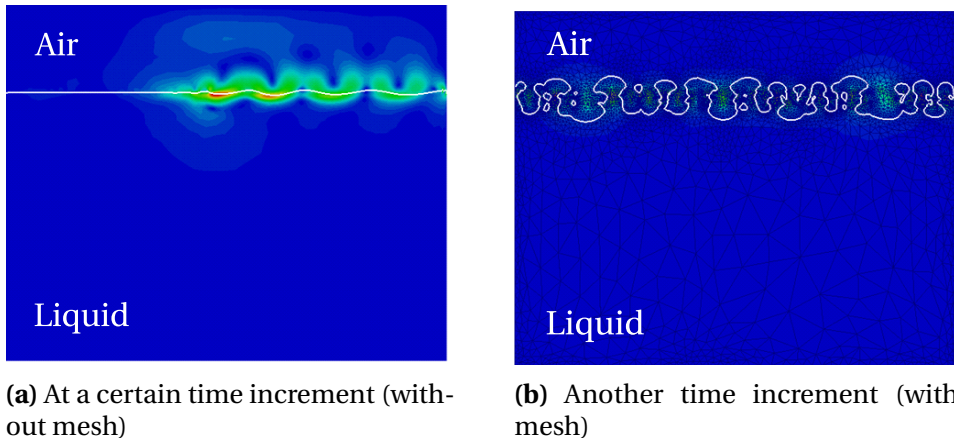


**Fig. 5.3** – Interface destabilisation under the effect of high properties ratio across the interface.

- satisfy the mass conservation principle, essentially in the metal.

We want to process the original transport velocity by imposing a uniform motion (speed and direction) at the nodes of the free surface, and at the same time, be able to follow the pipe formation at the surface as a result of solidification shrinkage, as shown in [fig. 5.4](#).

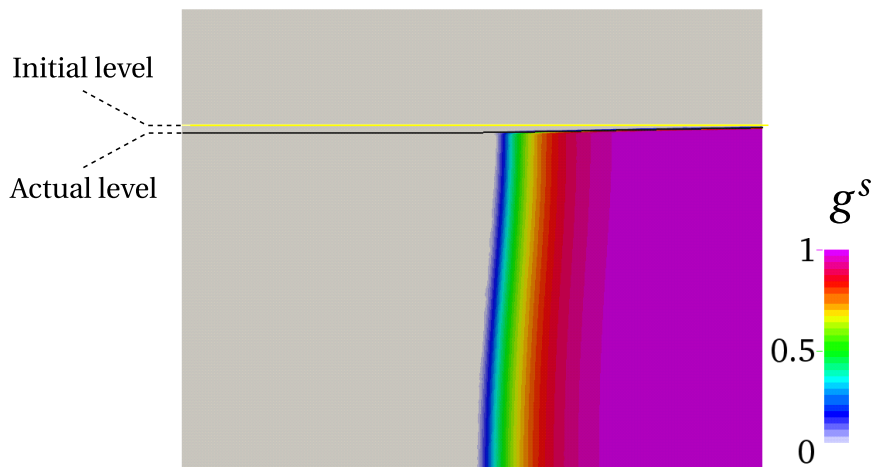


**Fig. 5.4** – Snapshot of a solidifying ingot by a cooling flux from the side. The profile of the actual surface changes in solid and mushy regions to adapt the new density while staying perfectly horizontal in the liquid phase.

How to transport level set using velocity from momentum conservation DIRECTLY or AVERAGED PER ELEMENTS, show examples of instability/stability when using false/nominal air properties

Validation of LS transport: perform test case simulation of buoyancy driven air droplet in water by 2005Nagragh that I also have seen in Shyamprasad's masters report). => I didnt notice: what time step  $\delta t$  did they use ?

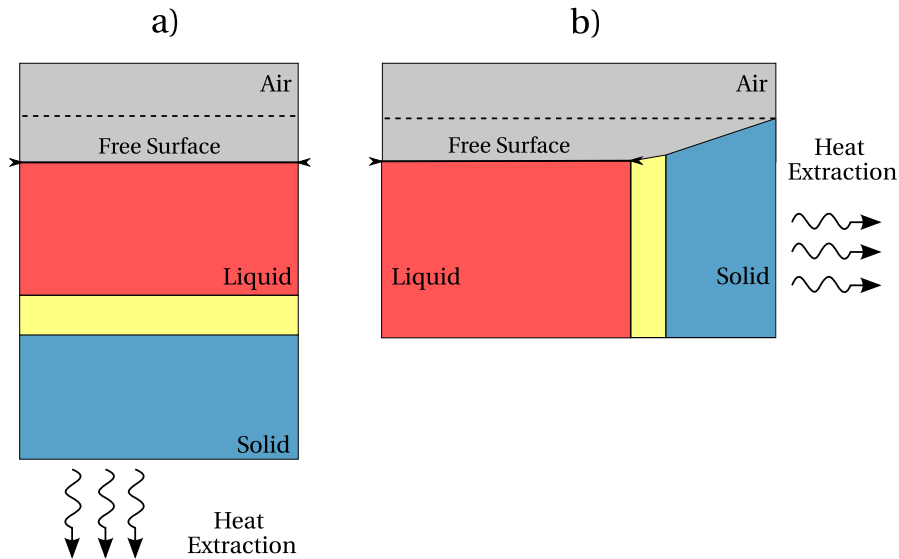


**Fig. 5.5** – Treatment of liquid free surface in a) bottom and b) side heat extraction configurations. The dashed line represents the initial level of the free liquid surface.

The general idea is read the velocity around the interface up to a certain thickness, which may be the same thickness as the diffuse interface defined in [section 2.4.1](#), then compute a volumetric average from all the elements in the thickness. This average is then given to the transport solver, which will apply the same magnitude and direction to transport the interface. However, as we only need the transport velocity to be uniform within the "100% liquid" elements, it should not be the case for the other elements that belong either to the mushy zone or the solid region, where shrinkage is taking place. Therefore, depending on the heat extraction configuration, two scenarios are possible. If heat extraction is far from the interface, i.e. there is not direct contact as in [fig. 5.5a](#), the surface area remains unchanged at any time, hence all the elements around the interface are "100% liquid". This happens when a bottom cooling is applied to the ingot. In contrast, if a side cooling is applied as shown in [fig. 5.5b](#), the surface area of the interface will be reduced over time as a consequence of the solid front progression. In this case, the average transport velocity should be computed only from the elements belonging to the free surface. The remaining part of the interface which belongs to partial or full solid regions, is transported with Navier-Stokes output, which should be some orders of magnitude less than the velocity imposed at the free surface, as a result of a decreasing permeability.

## 5.5 Shrinkage without macrosegregation

Explain how the flow and heat transfer in the air are not important

Give the strong form equations to be solved OR simply refer the previous section where

## **Chapter 5. Macrosegregation with solidification shrinkage**

---

the model was defined

Initial and boundary conditions for energy and momentum: Initially we have liquid and air at rest.

### **5.5.1 Al-7wt% Si**

Present pseudo 1D case with results + discussion

### **5.5.2 Pb-3wt% Sn**

Present 2D and 3D case with results + discussion

## **5.6 Shrinkage with macrosegregation**

Explain how the flow and heat transfer in the air are not important

Give the strong form equations to be solved OR simply refer the previous section where the model was defined

Initial and boundary conditions for energy and momentum: Initially we have liquid and air at rest.

### **5.6.1 Al-7wt% Si**

Present pseudo 1D case with results + discussion

### **5.6.2 Pb-3wt% Sn**

Present 2D and 3D case with results + discussion

# Bibliography

## [AFS 2014]

AFS (2014). *American Foundry Society: Understanding Porosity*. URL: <http://www.afsinc.org/about/content.cfm?ItemNumber=6933> (cited on page 3).

## [Beckermann 2002]

Beckermann, C. (2002). “Modelling of macrosegregation: applications and future needs”. *International Materials Reviews*, 47 (5), pp. 243–261. URL: <http://www.maneyonline.com/doi/abs/10.1179/095066002225006557> (cited on pages 5, 6).

## [Carozzani 2012]

Carozzani, T. (2012). “Développement d’un modèle 3D Automate Cellulaire-Éléments Finis (CAFE) parallèle pour la prédition de structures de grains lors de la solidification d’alliages métalliques”. PhD Thesis. Ecole Nationale Supérieure des Mines de Paris. URL: <http://pastel.archives-ouvertes.fr/pastel-00803282> (cited on page 10).

## [Combeau et al. 2009]

Combeau, H., Založnik, M., Hans, S., and Richy, P. E. (2009). “Prediction of Macrosegregation in Steel Ingots: Influence of the Motion and the Morphology of Equiaxed Grains”. *Metallurgical and Materials Transactions B*, 40 (3), pp. 289–304. URL: <http://link.springer.com/article/10.1007/s11663-008-9178-y> (cited on page 6).

## [Dantzig et al. 2009]

Dantzig, J. A. and Rappaz, M. (2009). *Solidification*. EPFL Press (cited on page 3).

## [Digonnet et al. 2007]

Digonnet, H., Silva, L., and Coupez, T. (2007). “Cimlib: A Fully Parallel Application For Numerical Simulations Based On Components Assembly”. *AIP Conference Proceedings*. Vol. 908. AIP Publishing, pp. 269–274. URL: <http://scitation.aip.org/content/aip/proceeding/aipcp/10.1063/1.2740823> (cited on page 11).

## [DLR 2014]

DLR (2014). *ElectroMagnetic Levitation*. <http://goo.gl/e5JhiA> (cited on page 10).

## [ESAB 2014]

ESAB (2014). *New Lean Duplex Steels*. URL: <http://www.esab.com/global/en/education/new-lean-duplex-steels.cfm> (cited on page 3).

## Bibliography

---

### [Felicelli et al. 1991]

Felicelli, S. D., Heinrich, J. C., and Poirier, D. R. (1991). "Simulation of freckles during vertical solidification of binary alloys". *Metallurgical Transactions B*, 22 (6), pp. 847–859. URL: <http://link.springer.com/article/10.1007/BF02651162> (cited on page 7).

### [Flemings 1974]

Flemings, M. C. (1974). "Solidification processing". *Metallurgical Transactions*, 5 (10), pp. 2121–2134. URL: <http://link.springer.com/article/10.1007/BF02643923> (cited on page 7).

### [Giamei et al. 1970]

Giamei, A. F. and Kear, B. H. (1970). "On the nature of freckles in nickel base superalloys". *Metallurgical Transactions*, 1 (8), pp. 2185–2192. URL: <http://link.springer.com/article/10.1007/BF02643434> (cited on page 7).

### [Gouttebroze 2005]

Gouttebroze, S. (2005). "Modélisation 3d par éléments finis de la macroségrégation lors de la solidification d'alliages binaires". PhD thesis. École Nationale Supérieure des Mines de Paris. URL: <https://pastel.archives-ouvertes.fr/pastel-00001885/document> (cited on page 10).

### [Lesoult 2005]

Lesoult, G. (2005). "Macrosegregation in steel strands and ingots: Characterisation, formation and consequences". *Materials Science and Engineering: A*, International Conference on Advances in Solidification Processes 413–414, pp. 19–29. URL: <http://www.sciencedirect.com/science/article/pii/S0921509305010063> (cited on page 7).

### [Liu 2005]

Liu, W. (2005). "Finite Element Modelling of Macrosegregation and Thermomechanical Phenomena in Solidification Processes". PhD thesis. École Nationale Supérieure des Mines de Paris. URL: <http://pastel.archives-ouvertes.fr/pastel-00001339> (cited on page 10).

### [Mesri et al. 2009]

Mesri, Y., Digonnet, H., and Coupez, T. (2009). "Advanced parallel computing in material forming with CIMLib". *European Journal of Computational Mechanics/Revue Européenne de Mécanique Numérique*, 18 (7-8), pp. 669–694. URL: <http://www.tandfonline.com/doi/abs/10.3166/ejcm.18.669-694> (cited on page 11).

### [Mosbah 2008]

Mosbah, S. (2008). "Multiple scales modeling of solidification grain structures and segregation in metallic alloys". PhD thesis. École Nationale Supérieure des Mines de Paris. URL: <https://tel.archives-ouvertes.fr/tel-00349885/document> (cited on page 10).

### [Rivaux 2011]

Rivaux, B. (2011). "Simulation 3D éléments finis des macroségrégations en peau induites par déformations thermomécaniques lors de la solidification d'alliages métalliques".

PhD Thesis. École Nationale Supérieure des Mines de Paris. URL: <http://pastel.archives-ouvertes.fr/pastel-00637168> (cited on page 10).

### [Sarazin et al. 1992]

Sarazin, J. R. and Hellawell, A. (1992). "Studies of Channel-Plume Convection during Solidification". *Interactive Dynamics of Convection and Solidification*. Ed. by S. H. Davis, H. E. Huppert, U. Müller, and M. G. Worster. NATO ASI Series 219. Springer Netherlands, pp. 143–145. URL: [http://link.springer.com/chapter/10.1007/978-94-011-2809-4\\_22](http://link.springer.com/chapter/10.1007/978-94-011-2809-4_22) (cited on page 4).

### [Schneider et al. 1997]

Schneider, M. C., Gu, J. P., Beckermann, C., Boettinger, W. J., and Kattner, U. R. (1997). "Modeling of micro- and macrosegregation and freckle formation in single-crystal nickel-base superalloy directional solidification". *Metallurgical and Materials Transactions A*, 28 (7), pp. 1517–1531. URL: <http://link.springer.com/article/10.1007/s11661-997-0214-3> (cited on page 4).

### [Shevchenko et al. 2013]

Shevchenko, N., Boden, S., Gerbeth, G., and Eckert, S. (2013). "Chimney Formation in Solidifying Ga-25wt pct In Alloys Under the Influence of Thermosolutal Melt Convection". *Metallurgical and Materials Transactions A*, 44 (8), pp. 3797–3808. URL: <http://link.springer.com/article/10.1007/s11661-013-1711-1> (cited on page 4).

### [Voller et al. 1989]

Voller, V. R., Brent, A. D., and Prakash, C. (1989). "The modelling of heat, mass and solute transport in solidification systems". *International Journal of Heat and Mass Transfer*, 32 (9), pp. 1719–1731. URL: <http://www.sciencedirect.com/science/article/pii/0017931089900549> (cited on page 98).

### [WeldReality 2014]

WeldReality (2014). *Aluminum Alloys*. URL: <http://www.weldreality.com/aluminumalloys.htm> (cited on page 3).

### [WSA 2014]

WSA (2014). *World Steel Association: Statistics archive*. URL: <http://www.worldsteel.org/statistics/statistics-archive.html> (cited on page 8).